Scripta Materialia 139 (2017) 104–107

Contents lists available at ScienceDirect

Scripta Materialia

journal homepage: www.elsevier.com/locate/scriptamat

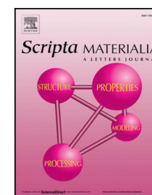

Regular article

PdGe contact fabrication on Se-doped Ge

M. Descoins [a], J. Perrin Toinin [a], S. Zhiou [a], K. Hoummada [a], M. Bertoglio [a], R. Ma [b], L. Chow [b], D. Narducci [c], A. Portavoce [a],*

[a] IM2NP, CNRS/Aix-Marseille University, Faculté des Sciences de Saint-Jérôme case 142, 13397 Marseille, France
[b] Department of Physics, University of Central Florida, Orlando, Florida 32816, USA
[c] Department of Materials Science, University of Milano-Bicocca, via R. Cozzi 55, 20125, Milano, Italy

ARTICLE INFO

Article history:
Received 22 December 2016
Received in revised form 12 June 2017
Accepted 15 June 2017
Available online xxxx

Keywords:
Germanium
Palladium
Selenium
Contact
Reaction

ABSTRACT

PdGe contact fabrication on Se-doped Ge(001) is investigated. PdGe thin film resistivity is two times lower if the PdGe layer is grown by Pd reactive diffusion on Se-doped Ge, compared to PdGe layer grown in the same condition on Se-free Ge. The phase sequence and the phase growth kinetics during Pd reactive diffusion with Ge are not modified by the presence of Se atoms. However, the PdGe film texture is different with Se, and Se segregates at the PdGe/Ge interface. These results suggest that Se atoms may be used to produce efficient contacts on *n*-type Ge.

© 2017 Acta Materialia Inc. Published by Elsevier Ltd. All rights reserved.

Si-based complementary metal oxide semiconductor (CMOS) technology development allowed continuous microelectronic device size reduction, combined with the continuous improvement of microelectronic device efficiency (speed, power consumption…). CMOS technology allows highly integrated, high-performance, and high-reliability microelectronic chips to be produced at relatively low-cost and high yield. To carry out this constant improvement, materials used to build and to connect transistors were changed or modified several times over the years from technology node to technology node. For example, Co was changed to Ni for silicide ohmic contacts [1–3], SiO_2 was changed to HfO_2 for gate dielectric [4–5], and Cu replaced Al for metallic interconnections [6–8]. Si was kept as the base semiconductor so far, but with the size limits insuring transistor standard operations soon being reached, different semiconductors other than Si should be used in future transistors in order to support device improvements [9–10]. Among them, Ge appears as a plausible choice, since Ge has faster charge carrier mobilities and is fully compatible with CMOS technology [11–16]. Ge was first introduced in the CMOS technology for heterojunction bipolar transistor fabrication, for low power high-frequency radio-frequency applications [17–19]. Today, complementary transistor technology uses *n*-type transistors with a Si channel stressed by SiGe source and drain, and *p*-type transistors with a SiGe channel [20–25]. In addition, Ge-based devices such as photodetectors are now integrated in Si photonics integrated circuits [26]. However, Ge-based CMOS technology suffers two major limitations: i) low *n*-type doping levels [27], and ii) the difficulty to produce ohmic contacts on *n*-type Ge [28–33]. PdGe is expected to be one of the best materials for ohmic contact fabrication on Ge due to its low resistivity and reduced Ge consumption [34]. Reactive diffusion of a thin Pd film on intrinsic Ge has been already studied aiming to design a self-aligned germanide process similar to the Salicide process used in Si CMOS technology [34–41]. Pd_2Ge was shown to grow first, and to be followed by the growth of PdGe. PdGe experiences an agglomeration process at relatively low temperature [39]. In the present work, the formation of a PdGe contact on *n*-type Se-doped Ge was investigated comparing with a PdGe film formed in the same condition on the same Ge substrate not doped with Se.

Ga-doped Ge(001) substrates exhibiting a resistivity between 0.059 and 0.088 Ω cm were implanted with a dose of 3.6×10^{15} Se at cm^{-2} with an energy of 130 keV, and annealed under vacuum (4×10^{-5} Torr) in a commercial rapid thermal annealing (RTA) setup at 700 °C for 30 min in order to activate Se atoms. Secondary ion mass spectrometry (SIMS) was used to determine the Se distribution in the sample using a CAMECA IMS 3F setup with a 3 keV O_2^+ ion beam, and Hall Effect electrical measurements were performed to measure the concentration of free carriers in the sample after activation. Then, a 20-nm thick polycrystalline Pd film was deposited at room temperature (RT) on the sample surface using a commercial magnetron sputtering system with a base pressure of 10^{-8} Torr. Pd was sputtered from a 99.99% pure Pd target using a 99.9999% pure Ar gas flow in the DC mode. Then, the sample was loaded in an X-ray diffraction (XRD) setup and was in situ annealed under vacuum (10^{-6} Torr) following a heating ramp consisted of 5 °C per minute steps separated by 5 min-

* Corresponding author.
E-mail address: alain.portavoce@im2np.fr (A. Portavoce).

http://dx.doi.org/10.1016/j.scriptamat.2017.06.029
1359-6462/© 2017 Acta Materialia Inc. Published by Elsevier Ltd. All rights reserved.

long XRD measurements at constant temperature (T), corresponding to an average ramp of ~1.7 °C min^{-1}. The XRD measurements were performed between RT and 400 °C in the Bragg-Brentano geometry, using a Cu K_α source ($\lambda_{K\alpha} = 0.154$ nm). XRD pole figures were also acquired at RT with steps of 2° after the in situ measurements using a focalized Cu K_α source. The atomic distribution in the sample was analyzed by atom probe tomography (APT) after annealing using a CAMECA LEAP 3000X-HR system. APT measurements were performed in the laser mode at $T = 20$ K with a laser energy of 0.15 nJ, a laser pulse frequency of 100 kHz, and an evaporation rate of 0.2%. The PdGe film resistivity was measured using the four probe technique and compared to the resistivity of a PdGe film grown in the same condition on the same Ge substrate but not doped with Se. The PdGe resistivity (ρ) was averaged over 15 measurements performed on different locations on the same film.

Fig. 1 presents the Se SIMS profiles measured in the Ge(001) substrate after Se implantation (open triangles) and after the activation annealing performed at 700 °C for 30 min (open squares). The Se distribution corresponds to a Gaussian distribution after implantation, with a maximum concentration of ~5×10^{20} at cm^{-3} located at ~60 nm below the sample surface. Se atoms diffused during activation annealing, decreasing this maximum to ~1×10^{20} at cm^{-3}. The average doping level measured in this sample by the Hall effect technique was found to be ~3.3×10^{19} electrons cm^{-3}, which corresponds to a Ge resistivity of ~7.7×10^2 μΩ cm [42]. One note that Se atoms being considered as double donors [43], the electron concentration is expected to correspond to an average Se concentration of only ~1.65×10^{19} at cm^{-3} that is close to our APT detection limit [44–46]. Se concentrations higher than this limit correspond to inactive Se atoms, probably incorporated in Se-Ge clusters. Fig. 2a displays the evolution of the diffractogram measured in situ versus T during the ramp annealing of the [20-nm thick Pd/Se-doped Ge(001)] sample. As expected [37–38, 40], the phase formation sequence is sequential with the formation of only two phases: first Pd_2Ge and second PdGe. A single diffraction peak is detected after Pd deposition at the diffraction angle 2θ ~ 40°, corresponding to the Pd(111) atomic planes. The diffraction intensity of this peak decreases during annealing until total extinction, while the intensity of the Pd_2Ge(111) and Pd_2Ge(002) peaks (2θ ~ 37.5° and 53.7°, respectively) increases simultaneously from zero up to a maximum, resulting from the Pd layer consumption during the Pd_2Ge layer growth. Similarly, the consumption of the Pd_2Ge layer during the growth of PdGe leads to the decrease of Pd_2Ge(111) and Pd_2Ge(002) peak intensities, with the concomitant intensity increase of five new peaks corresponding to PdGe (2θ ~ 29.3°, 33.2°, 41.7°, 43°, and 52.5°, consistent with PdGe (101), (111), (211), (121), and (002) planes, respectively). A single PdGe layer is in contact with the Ge substrate at the end of the experiment. The observed diffraction peaks of all the phases are similar to those observed during the reaction of a Pd film on a Se-free Ge(001) substrate [41]. Fig. 2b and c present the variation versus T of integrated and normalized diffraction peaks corresponding to the most intense peak of each phase present in the phase sequence with and without Se: the Pd(111), Pd_2Ge(002), and the PdGe(101) peaks. Based on the Pd(111) peak decrease, Pd_2Ge growth is observed to start at T ~ 115 °C with Se, which is similar to the case of Pd reaction on the Se-free Ge substrate [40]. PdGe growth starts at T ~ 225 °C, which is close to what is observed with the Se-free Ge substrate [40]. Fig. 3a presents XRD measurements performed at RT after annealing, on the PdGe layer grown on the Se-doped substrate (open squares), as well as on a PdGe layer grown in the same conditions on a Se-free substrate (open circles). The main diffraction peaks are the same for the two samples. The most intense diffraction peaks correspond to the PdGe (101) and (111) planes. These planes do not exhibit the highest XRD structure factor (41% and 48.5%, respectively). Consequently, these diffractograms do not correspond to an entirely random texture. The texture of the PdGe layers was investigated using XRD pole figure measurements performed for the PdGe (211), (121), and (101) planes. Fig. 3b and c present the (121) pole figures obtained on the samples with and without Se, respectively. A random-like signal is detected in the two cases (background intensity in Fig. 3b and c). However, the measurements show that the strongest diffraction intensity results from the axiotaxial texture PdGe(121)//Ge(220) in the Se-free sample, while it corresponds to the epitaxial texture PdGe(001)//Ge(001) in the sample with Se. These two types of texture were already reported between PdGe and Ge [47]. Consequently, Se doping does not modify the phase sequence and the phase growth kinetics during Pd reaction with the Ge substrate, but promotes an epitaxial texture instead of an axiotaxial texture. The resistivity measurements performed on the PdGe films grown either on the Se-doped Ge substrate or the Se-free Ge substrate show significant differences. The resistivity of the PdGe film grown on the Se-

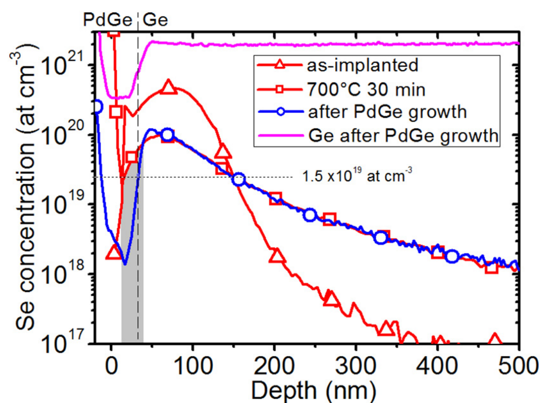

Fig. 1. Se SIMS profiles measured in the Se-implanted Ge(001) substrate before (open triangles) and after (open squares) activation annealing, as well as in the PdGe/Se-doped Ge sample after an annealing ramp of ~1.7 °C min^{-1} up to 400 °C (open circles).

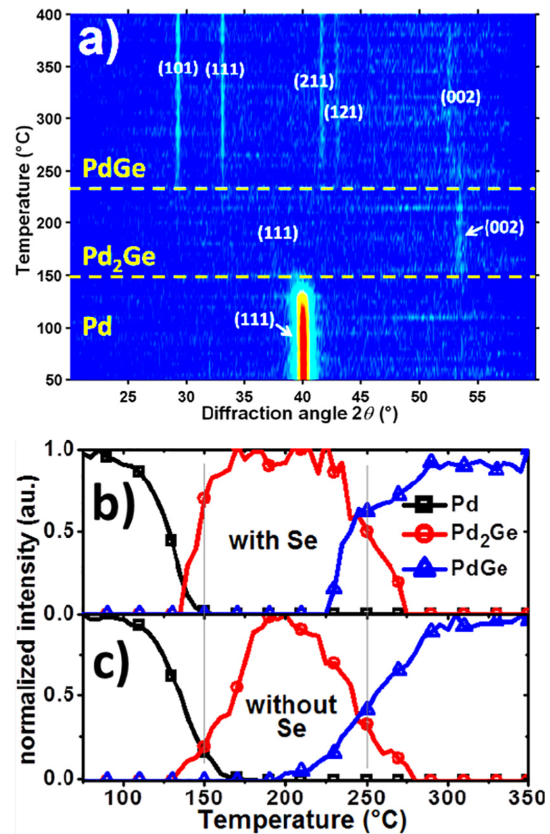

Fig. 2. a) In situ XRD measurements performed on the Se-doped sample; b) and c) integrated and normalized Pd(111), Pd_2Ge(002) and PdGe(101) diffraction peaks recorded during in situ XRD annealing of a Pd layer deposited either on a Se-doped Ge substrate (b) or on a Se-free Ge substrate (c).

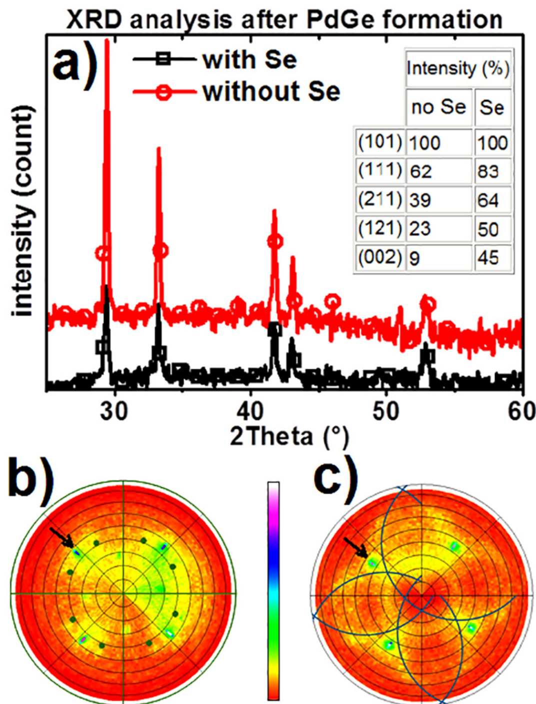

	Intensity (%)	
	no Se	Se
(101)	100	100
(111)	62	83
(211)	39	64
(121)	23	50
(002)	9	45

Fig. 3. a) Diffractograms (a) and pole figures measured at RT in a PdGe layer grown either on a Se-doped Ge substrate (b) or on a Se-free Ge substrate (c). The inset in fig. a presents peak intensity ratios normalized to the (101) diffraction peak intensity. The four poles observed in fig. b and c (black arrow) correspond to the Ge{220} plane diffraction. The solid circles in fig. b highlight the eight poles resulting from the epitaxial texture PdGe(001)//Ge(001). The solid lines in fig. c highlight the signal corresponding to the axiotaxial texture PdGe(121)//Ge(220).

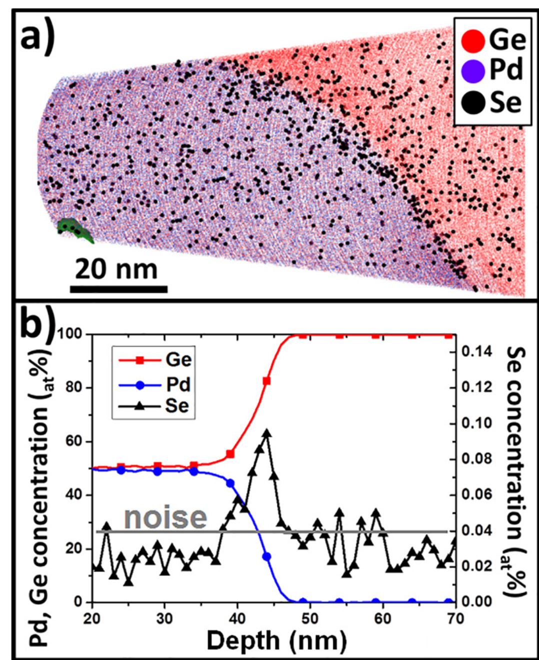

Fig. 4. APT measurements performed on the [Pd/Se-doped Ge(001)] sample after in situ XRD annealing: a) side view of the entire 60 × 60 × 110 nm^3 APT volume; and b) 1D concentration profiles measured perpendicularly to the PdGe/Ge interface in the volume presented in a).

doped Ge substrate was found to be $\rho = 6 \pm 0.8$ μΩ cm, which is two times smaller than $\rho = 13 \pm 1$ μΩ cm measured on the PdGe film grown on the Se-free Ge substrate. This result is of high interest since ohmic contact on *n*-type Ge has not been yet demonstrated. The Se distribution measured by SIMS after PdGe formation is presented in Fig. 1 (open circles). The depth of the PdGe/Ge interface was set at ~30 nm, since the reaction of 20 nm of Pd consumed about 30 nm of Ge in order to form a ~45 nm-thick PdGe layer. The maximum Se concentration is located at the PdGe/Ge interface, showing a slight Se accumulation up to ~1.2 × 10^{20} at cm^{-3} compared to the profile measured before PdGe growth (open squares). The comparison between these two profiles shows also that Se atoms did not diffuse in Ge bulk during the annealing ramp. The Se profile measured in PdGe (not calibrated) shows the presence of a Se gradient from the surface up to the PdGe/Ge interface. For comparison, the uncalibrated Ge profile measured in the PdGe layer forms a plateau (Fig. 1), as expected. The sample was also analyzed by APT. Fig. 4a presents an APT volume analyzed in the sample after XRD in situ annealing up to 400 °C (Fig. 2), focusing specifically the PdGe/Ge interface. Each dot is a single atom, red, blue, and black dots corresponding to Ge, Pd, and Se atoms, respectively. Se atoms are observed at both sides of the interface. However, a Se atom accumulation is clearly observed at the PdGe/Ge interface. Fig. 4b presents one-dimensional (1D) Ge, Pd, and Se concentration profiles measured in the volume presented in Fig. 4a in the direction perpendicular to the PdGe/Ge interface. As expected, the Pd and Ge concentrations correspond to 50 at% in the PdGe layer, and allow the PdGe/Ge interface to be clearly determined in the APT profiles. However, the Se concentration profile in PdGe and Ge could not be determined by APT. Indeed, the study of the mass spectrum (not shown) in both side of the PdGe/Ge interface showed that the Se atoms detected in the PdGe and the Ge volumes correspond to the noise level of APT measurements (~0.9–1.8 × 10^{19} at cm^{-3}, see Fig. 4b). Thus, the Se bulk concentration in the PdGe/Ge interface vicinity is found to be similar (or lower) to the concentration of activated Se atoms before Pd/Ge reaction, Hall effect measurements performed before PdGe growth expecting an activated Se concentration in Ge lower than 2 × 10^{19} at cm^{-3}. Though, the Se APT profile shows clearly the Se segregation at the interface between the contact layer and the semiconductor, with a Se interfacial concentration of ~0.09%, corresponding to ~4 × 10^{19} Se at cm^{-3} in Ge. However, atomic distributions measured at interfaces by APT are known to be artificially spread out. Thus, the quantitative Se concentration located at the PdGe/Ge interface should be calculated from the detected segregation peak integration. The integration of the Se segregation peak located at the PdGe/Ge interface gives a total Se dose of ~0.67% nm. Considering that the interface thickness is similar to that of grain boundaries (0.5 nm), the Se interfacial concentration is found to be ~0.335%, which corresponds to ~1.5 × 10^{20} at cm^{-3} in Ge, in good agreement with SIMS measurements. The fact that, contrasting with SIMS measurements, no Se atoms were detected in Ge in the PdGe/Ge interface vicinity in APT measurements could be related to the formation of Se-Ge clusters (as suggested by Hall effect measurements) exhibiting low bulk density, significantly reducing the probability to observe one of these clusters in an APT volume (field of view ~60 × 60 nm^2 compared to ~60 × 60 μm^2 for SIMS). Se was shown to passivate the Ge(001) surface [48]. Thus, Se segregation at Ge interfaces is expected to modify Ge interface electronic properties, decreasing charge carrier recombination for example. Consequently, the PdGe resistivity decrease observed on Se-doped Ge substrate could be due to the Se segregation detected at the PdGe/Ge interface. The segregated Se dose of ~0.67% nm corresponds to 2.97 × 10^{13} at cm^{-2} and to ~0.05 atomic monolayer (ML), considering the Ge bulk density (4.42 × 10^{22} at cm^{-3}) as reference. 0.05 ML seems quite low for interface passivation, if the interface between PdGe and Ge is not partially coherent. It is interesting to note that the Se dose integrated in the region of the SIMS profile measured before Pd reaction (open squares in Fig. 1) corresponding to the 30 nm-thick Ge consumed to form the PdGe layer (gray region in Fig. 1) is ~9.2 × 10^{13} at cm^{-2}. This value is about three times higher than the Se dose measured at the PdGe/Ge interface. Due to the annealing temperature (T < 400 °C during ~3.5 h), Se is expected to have entered the polycrystalline PdGe layer thanks to grain boundary (GB) diffusion

[49], GB diffusion being generally about four orders of magnitude faster than lattice diffusion [50]. Despite that APT analyses did not allow the observation of GBs in the PdGe layer, SIMS measurements show a Se gradient in the PdGe layer (open circles in Fig. 1) that could support this assumption. Thus, one cannot exclude that the resistivity decrease in the PdGe layer grown on Se-doped Ge could also result from Se diffusion and segregation in PdGe GBs.

In conclusion, the fabrication of a PdGe germanide contact on *n*-type Se-doped Ge(001) was investigated, using standard CMOS processes. Electrical measurements show that the PdGe film resistivity is significantly reduced compared with PdGe films grown in the same condition on Se-free Ge substrate. SIMS and APT measurements suggest that the Se influence on PdGe film resistivity results from Se segregation at the PdGe/Ge interface. These results show that Se can be used to create improved metallic contacts on *n*-type Ge. They also confirm that the choice of materials (such as PdGe) for ohmic contact fabrication cannot be only based on their bulk resistivity, but should also include dopants, since they can have a significant effect on contact resistivity. For example, NiGe resistivity is about 2/3 of PdGe resistivity [34], while, on Se-doped Ge, PdGe resistivity becomes 3/4 of NiGe resistivity.

This work was supported by the French National Agency for Research (ANR) through the program “Science de l'ingénierie” (Project DoGeTec, no. ANR-12-JS09-0015-1).

References

[1] A. Lauwers, A. Steegen, M. de Potter, R. Lindsay, A. Satta, H. Bender, K. Maex, J. Vac. Sci. Tech. B 19 (2001) 2026.
[2] J.A. Kittl, A. Lauwers, O. Chamirian, M. Van Dal, A. Akheyar, M. De Potter, R. Lindsay, K. Maex, Microelectron. Eng. 70 (2003) 158.
[3] C. Lavoie, F.M. d'Heurle, C. Detavernier, C. Cabral Jr., Microelectron. Eng. 70 (2003) 144.
[4] G.D. Wilk, R.M. Wallace, J.M. Anthony, J. Appl. Phys. 89 (2001) 5243.
[5] R. Gupta, R. Rajput, R. Prasher, R. Vaid, Solid State Sci. 59 (2016) 7.
[6] C.-K. Hu, B. Luther, F.B. Kaufman, J. Hummel, C. Uzoh, D.J. Pearson, Thin Solid Films 262 (1995) 84.
[7] S.P. Hau-Riege, AIP Conf. Proc. 612 (2002) 21.
[8] L.C. Leu, D.P. Norton, L. McElwee-White, L.C. Leu, T.J. Anderson, Appl. Phys. Lett. 92 (2008) 111917.
[9] J.A. del Alamo, Nature 479 (2011) 317.
[10] S. Takagi, S.-H. Kim, M. Yokoyama, R. Zhang, N. Taoka, Y. Urabe, T. Yasuda, H. Yamada, O. Ichikawa, N. Fukuhara, M. Hata, M. Takenaka, Solid-State Elec. 88 (2013) 2.
[11] G. Hock, T. Hackbarth, U. Erben, E. Kohn, U. Konig, Electron. Lett. 34 (1998) 1888.
[12] A. Toriumi, T. Tabata, C.H. Lee, T. Nishimura, K. Kita, K. Nagashio, Microelectron. Eng. 86 (2009) 1571.
[13] R. Pillarisetty, B. Chu-Kung, S. Corcoran, G. Dewey, J. Kavalieros, H. Kennel, R. Kotlyar, V. Le, D. Lionberger, M. Metz, N. Mukherjee, J. Nah, W. Rachmady, M. Radosavljevic, U. Shah, S. Taft, H. Then, N. Zelick, R. Chau, IEEE Int. Electron Devices Meet. 150 (2010).
[14] K.J. Kuhn, M.Y. Liu, H. Kennel, IEEE Int. Workshop Junct. Technol. (2010) 1.
[15] C. Le Royer, Microelectron. Eng. 88 (2011) 1541.
[16] C.H. Fu, Y.H. Lin, W.C. Lee, T.D. Lin, R.L. Chu, L.K. Chu, P. Chang, M.H. Chen, W.J. Hsueh, S.H. Chen, G.J. Brown, J.I. Chyi, J. Kwo, M. Hong, Microelectron. Eng. 147 (2015) 330.
[17] L.E. Larson, J. Vac. Sci. Technol. B 16 (1998) 1541.
[18] K. Washio, in: Y. Shiraki, N. Usami (Eds.), Silicon–Germanium (SiGe) Nanostructures, Woodhead Publishing, Oxford 2011, p. 473 Part IV.
[19] G.G. Fischer, G. Sasso, Microelec. Reliability 55 (2015) 498.
[20] W.-C. Wang, S.-T. Chang, J. Huang, S.-J. Kuang, Solid-State Elec. 53 (2009) 880.
[21] S. Takagi, Y. Shiraki, N. Usami, Silicon–Germanium (SiGe) Nanostructures, Woodhead Publishing, Oxford, 2011 499 Part IV.
[22] C. Reichel, J. Schoenekess, S. Kronholz, G. Beernink, A. Zeun, A. Dietel, T. Kammler, Thin Solid Films 520 (2012) 3170.
[23] K.E. Kambour, C. Kouhestani, P. McMarr, H.L. Hughes, D.R. Steinke, R.A.B. Devine, J. Vac. Sci. Technol. B 33 (2015), 022201. .
[24] A. Hikavyy, E. Rosseel, S. Kubicek, G. Mannaert, P. Favia, H. Bender, R. Loo, N. Horiguchi, Thin Solid Films 602 (2016) 72.
[25] R. Estivill, PhD thesis 2016.
[26] D. Thomson, A. Zilkie, J.E. Bowers, T. Komljenovic, G.T. Reed, L. Vivien, D. Marris-Morini, E. Cassan, L. Virot, J.-M. Fédéli, J.-M. Hartmann, J.H. Schmid, D.-X. Xu, F. Boeuf, P. O'Brien, G.Z. Mashanovich, M. Nedeljkovic, J. Opt. 18 (2016), 073003. .
[27] E. Simoen, M. Schaekers, J. Liu, J. Luo, C. Zhao, K. Barla, N. Collaert, Phys. Status Solidi A (2016) 1.
[28] J.A. Kittl, K. Opsomer, C. Torregiani, C. Demeurisse, S. Mertens, D.P. Brunco, M.J.H. Van Dal, A. Lauwers, Mater. Sci. Eng. B 154–155 (2008) 144.
[29] A. Chawanda, C. Nyamhere, F.D. Auret, W. Mtangi, M. Diale, J.M. Nel, J. Alloys and Compounds 492 (2010) 649.
[30] K. Martens, A. Firrincieli, R. Rooyackers, B. Vincent, R. Loo, S. Locorotondo, E. Rosseel, T. Vandeweyer, G. Hellings, B.D. Jaeger, M. Meuris, P. Favia, H. Bender, B. Douhard, J. Delmotte, W. Vandervorst, E. Simoen, G. Jurczak, D. Wouters, J.A. Kittl, Tech. Dig. - Int. Electron Devices Meet (2010) 428.
[31] K. Martens, R. Rooyackers, A. Firrincieli, B. Vincent, R. Loo, B. De Jaeger, M. Meuris, P. Favia, H. Bender, B. Douhard, W. Vandervorst, E. Simoen, M. Jurczak, D.J. Wouters, J.A. Kittl, Appl. Phys. Lett. 98 (2011), 013504. .
[32] A. Firrincieli, K. Martens, R. Rooyackers, B. Vincent, A. Firrincieli, K. Martens, R. Rooyackers, B. Vincent, E. Rosseel, E. Simoen, J. Geypen, H. Bender, C. Claeys, J.A. Kittl, Appl. Phys. Lett. 99 (2011) 242104.
[33] V. Janardhanam, J.-S. Kim, K.-W. Moon, K.-S. Ahn, C.-J. Choi, Microelectron. Eng. 89 (2012) 10.
[34] S. Gaudet, C. Detavernier, A. Kellock, P. Desjardins, C. Lavoie, Vac. Sci. Technol. A 24 (2006) 474.
[35] G. Ottaviani, C. Canali, G. Ferrari, R. Ferrari, G. Majni, M. Prudenziati, S. Lau, Thin Solid Films 47 (1977) 187.
[36] F. Nava, G. Majni, G. Ottaviani, Thin Solid Films 77 (1981) 319.
[37] C.M. Comrie, D. Smeets, K.J. Pondo, C. van der Walt, J. Demeulemeester, W. Knaepen, C. Detavernier, A. Habanyama, A. Vantomme, Thin Solid Films 526 (2012) 261.
[38] F. Greenen, W. Knaepen, K. De Keyser, K. Opsomer, R. Varmeirhaeghe, J. Jordan-Sweet, C. Lavoie, C. Detavernier, Thin Solid Films 551 (2014) 86.
[39] J. Perrin Toinin, K. Hoummada, M. Bertoglio, A. Portavoce, Scripta Mat. 120 (2016) 45.
[40] J. Perrin Toinin, K. Hoummada, M. Bertoglio, A. Portavoce, Scripta Mat. 122 (2016) 22.
[41] J. Perrin Toinin, A. Portavoce, M. Texier, M. Bertoglio, K. Hoummada, Microelectron. Eng. 167 (2017) 52.
[42] D.B. Cuttriss, Bell Syst. Tech. J. (1961) 509.
[43] H.G. Grimmeiss, L. Montelius, K. Larsson, Phys. Rev. B 37 (1988) 6916.
[44] A. Portavoce, I. Blum, D. Mangelinck, K. Hoummada, L. Chow, V. Carrond, J.L. Lábár, Scripta Mat. 64 (2011) 828.
[45] A. De Luca, A. Portavoce, M. Texier, C. Grosjean, N. Burle, V. Oison, B. Pichaud, J. Appl. Phys. 115 (2014), 013501. .
[46] A. De Luca, M. Texier, A. Portavoce, N. Burle, C. Grosjean, S. Morata, F. Michel, J. Appl. Phys. 117 (2015) 115302.
[47] F.A. Geenen, W. Knaepen, K. De Keyser, K. Opsomer, R.L. Vanmeirhaeghe, J. Jordan-Sweet, C. Lavoie, C. Detavernier, Thin Solid Films 551 (2014) 86.
[48] R.K. Chellappan, G. Hughes, Phys. Status Solidi (RRL) 7 (2013) 590.
[49] A. Portavoce, K. Hoummada, F. Dahlem, Surf. Sci. 624 (2014) 135.
[50] A. Portavoce, L. Chow, J. Bernardini, Appl. Phys. Lett. 96 (2010) 214102.